Title: ELECTRICAL BEHAVIOR OF $BaSnO_3$ BULK SAMPLES FORMED BY SLIP CASTING: EFFECT OF SYNTHESIS METHODS USED FOR OBTAINING THE CERAMIC POWDERS

Author: Y.H. Ochoa F. Schipani C.M. Aldao M.A. Ponce R. Savu J.E. Rodríguez-Páez

PII: S0025-5408(16)30091-5
DOI: http://dx.doi.org/doi:10.1016/j.materresbull.2016.02.037
Reference: MRB 8683

To appear in: *MRB*

Received date: 15-11-2015
Revised date: 17-2-2016
Accepted date: 22-2-2016

Please cite this article as: Y.H.Ochoa, F.Schipani, C.M.Aldao, M.A.Ponce, R.Savu, J.E.Rodríguez-Páez, ELECTRICAL BEHAVIOR OF BaSnO3 BULK SAMPLES FORMED BY SLIP CASTING: EFFECT OF SYNTHESIS METHODS USED FOR OBTAINING THE CERAMIC POWDERS, Materials Research Bulletin http://dx.doi.org/10.1016/j.materresbull.2016.02.037

ELECTRICAL BEHAVIOR OF $BaSnO_3$ BULK SAMPLES FORMED BY SLIP CASTING: EFFECT OF SYNTHESIS METHODS USED FOR OBTAINING THE CERAMIC POWDERS

Y.H. Ochoa[1]F. Schipani[2], C.M. Aldao[2], M.A. Ponce[2], R. Savu[3]*, J.E. Rodríguez–Páez[1]

[1]CYTEMAC Group, University of Cauca, Popayán, Colombia.

[2]Institute of Materials Science and Technology (INTEMA), University of Mar del Plata and National Research Council (CONICET), Juan B. Justo 4302, B7608FDQ Mar del Plata, Argentina

[3]Center for Semiconductor Components, Campinas State University, Rua João Pandiá Calogeras 90, 13083-870, Campinas, SP, Brazil.

***Corresponding author:** rsavu@unicamp.br; telephone +55 19 32517282

Graphical abstract

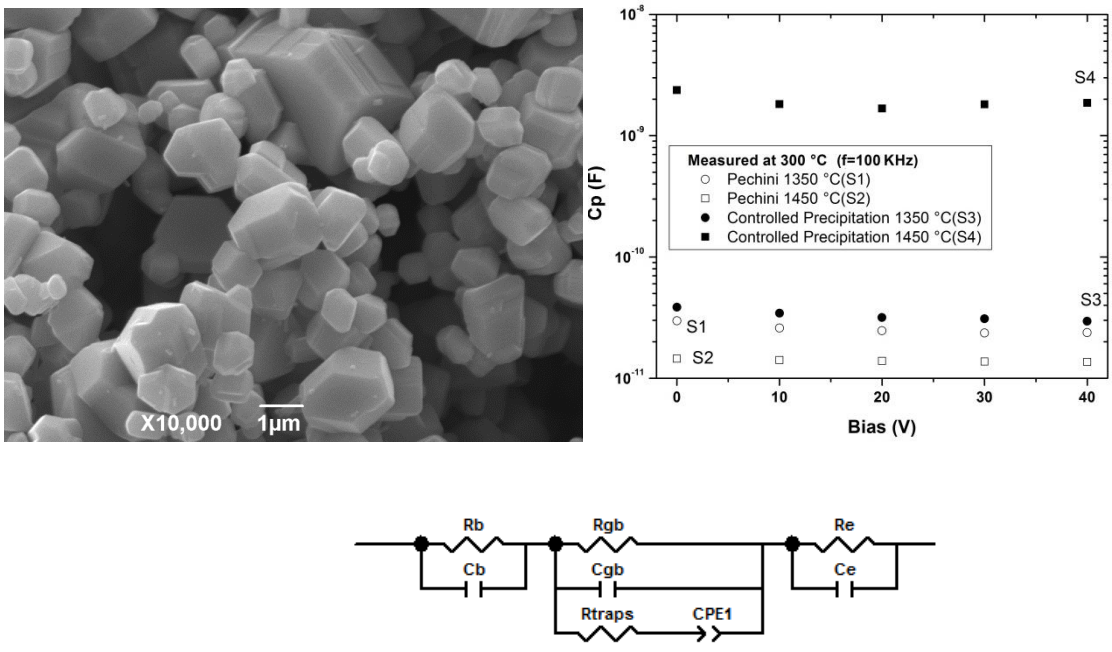

Highlights:

- Barium stannate ($BaSnO_3$) ceramic powders were synthesized using two chemical methods (controlled precipitation and Pechini);
- Comparison of the electrical behavior in air at 300 °C for pieces sintered using a range of temperatures;
- The method of synthesis has strong effects on the electrical behavior of the sintered samples.

Abstract

In order to build bulk pieces using the slip casting technique, barium stannate ($BaSnO_3$) ceramic powders were synthesized using two chemical methods (controlled precipitation and Pechini). Differences in the electrical behavior of the pieces, depending on the synthesis method employed, were then determined. For the analysis, a stable suspension of the synthesized ceramic powder (or 57.6 % solids slip) was obtained using water as solvent; the slip was poured into a mold to produce parallelepiped shaped green pieces. The electrical behavior in air at 300 °C was determined for pieces sintered using a range of temperatures. The results of this electrical characterization showed that the method of synthesis has strong effects on the electrical behavior of the sintered samples.

Keywords: ceramics, chemical synthesis, electron microscopy, electrical properties, impedance spectroscopy, defects.

1. Introduction

In the $BaO–SnO_2$ binary system, three compounds, in particular, can be obtained: $BaSnO_3$, $Ba_3Sn_2O_7$ and Ba_2SnO_4, the first of these being the best known, most widely studied and most useful. $BaSnO_3$ features a cubic perovskite type structure [1] and is a compound widely used in technological applications due to its dielectric properties, for example as a transparent conductor and to built capacitors, varistors, electrocatalytic electrodes, photovoltaic cells, and gas sensors [2, 3]. Particular features of this perovskite, and hence the interest in it, are principally related to the easy modification of its electrical properties and its high temperature stability. As a gas sensor, $BaSnO_3$ is a very promising material for high–temperatures detection [4]; in particular those temperatures are reached in the combustion processes.

The synthesis of the $BaSnO_3$ ceramic powders is carried out using a number of methods including sol–gel, co–precipitation of oxalates or hydroxides, hydrothermal process, and solid–state reactions [5, 6]. Due to modern-day requirements and with the aim of improving the functionality of the ceramic pieces (for example, gas sensor applications) the correct forming of synthesized $BaSnO_3$ powders is essential for obtaining sintered parts with the required densification, suitable microstructure and/or high mechanical properties, depending on their potential use. Regarding the formation process of the ceramic pieces, a first generation of gas sensors was prepared using thick film technology, for example screen printing, using ceramic powders. This process is not easily reproducible, given that the sensor behavior depends on percolation by means of intergranular resistance, a parameter that varies considerably according to the smallest details of the preparation process. Subsequently, the fabrication process was improved using thin film technology, applying both physical (evaporation or sputtering) and chemical (chemical vapor deposition) methods. However, this improvement in the technology of device production had the effect of reducing the sensitivity of the active material due to the lower porosity of the films. Efforts are currently being made to increase the homogeneity of the microstructure of the green pieces and their densification, making use of different techniques. Among these, slip casting stands out, and as such is the technique chosen for use in this work [7].

For making ceramic pieces by casting, small particles colloidal suspensions of the compound of interest are used (in this case $BaSnO_3$), and stabilized in a solvent, usually water, in the presence of a deflocculant. Therefore, the appropriate dosage of additives and solid ($BaSnO_3$ powders) in the starting suspension needs to be determined, with the aim of obtaining a suitably stable slip with good rheological properties for casting the pieces [8]. While colloidal forming is a widely used technique [7, 9–11] due to its versatility, only recently has it begun to be used, with enormous potential, in the formation of suspensions containing nanoparticles [12–15].

The forming method used in producing a ceramic piece clearly affects its electrical behavior, since the method employed determines its microstructural characteristics such as densification, porosity, and grain size, characteristics that in the case of gas sensors are crucially important as they determine the device sensor capacity.

In this work we used $BaSnO_3$ ceramic powders synthesized by two chemical methods (controlled precipitation and polymer precursor - Pechini) to obtain bulk ceramic pieces using the slip casting technique, with ammonium polyacrylate ($PAA–NH_4$) as deflocculant. Then, the pieces obtained were subjected to heat treatments at different temperatures to modify their microstructural characteristics.

Finally, the samples were characterized using the technique of complex impedance to study their electrical behavior and determine the effect of the synthesis method on their electrical characteristics.

2. Experimental procedure

2.1. $BaSnO_3$ synthesis by the Pechini method

To obtain $BaSnO_3$ by the Pechini method, a mixture of ethylene glycol and citric acid was first heated to 70 °C. The precursors $C_4H_6BaO_4$ and $SnCl_2.2H_2O$, in the amounts 8.4 and 7.4 g, respectively, were added to the ethylene glycol and citric acid solution. The resulting solution was brought to a basic pH and heated to 140 °C, stirring constantly until a resin was formed. The resin was then pre–calcined at 350 °C and, subsequently, subjected to a heat treatment at 1000 °C to obtain the $BaSnO_3$ material. The powder obtained at the end of the synthesis processes was characterized by X–Ray Diffraction (XRD) and Scanning Electron Microscopy (SEM) [16].

2.2. $BaSnO_3$ synthesis by the controlled precipitation method

To obtain the $BaSnO_3$ using the controlled precipitation method, $SnCl_2.2H_2O$ and $C_4H_6BaO_4$ were used as precursors. These were dissolved separately in 0.1M aqueous HNO_3 solutions. The suspensions obtained were then mixed and the obtained product was left to age. Finally, the suspension was washed with an aqueous solution of diethylamine. The wet solid obtained was dried at 100 °C and, in due course, was treated at 1250 °C for 2 hours. The final powder was ground in an agate mortar before being characterized [16].

2.3. Forming of ceramic pieces

In the forming of ceramics pieces by the colloidal method, calculations were made to determine the proportions of water and solid material required in order to guarantee certain "ideal" conditions in the suspension (slip density of 2.1 g/cm^3 [5]). The calculations performed gave rise to suspensions of 57.6 % by weight of solids – ceramic powders synthesized by the controlled precipitation method. Ammonium polyacrylate (PAA–NH_4) was used as a deflocculant. When the dispersion process was complete, the slip was poured into the mold. This mold was formed by taking 75 g of water per 100 g of gypsum (consistency 75) according to the requirements set by international standards [16]. The slip was poured into the mold and left until it reached the desired wall size, and then the piece was removed. Sintering of the samples was performed in a Carbolite furnace model RHF 1600. The formed

pieces were subjected to heat treatments at temperatures of 1350 and 1450 °C for 3 hours and characterized using SEM.

2.4. Electrical characterization

In order to determine the electrical behavior (in air atmosphere) of the sintered ceramic pieces a HP4284A impedance analyzer was used. The measurements were carried out at a frequency interval from 20 Hz to 1 MHz. Resistance and capacitance vs. frequency measurements were carried out at 300°C. A Novocontrol BDS 1200 commercial temperature controller was used to heat the samples to different temperatures.

3. Results and discussions

3.1. Characterization of synthesized powders

The diffractograms in Figure 1 show samples synthesized with the Pechini method (PDF 89–2488) obtained at 1000 °C, a lower temperature than the 1250 °C required in the controlled precipitation method to obtain the same compound (PDF 15-780).

Figure 2 shows the SEM micrographs corresponding to the $BaSnO_3$ ceramic powders obtained using controlled precipitation, thermally treated at 1250 °C (Fig. 2 (a)), and Pechini method, treated at 1000 °C (Fig. 2 (b)). Images demonstrate the presence of polyhedral agglomerates larger than 1μm (Fig. 2 (a)), and cubic agglomerates larger than 5 μm (Fig. 2 (b)).

3.2. Characterization of $BaSnO_3$ ceramic pieces formed by slip casting

Figure 3 shows the SEM micrographs of the surface microstructure for the ceramic pieces sintered at different temperatures (S1 and S3 at 1350 °C, S2 and S4 at 1450 °C). Figs. 3(a) and 3(b) depict those formed with $BaSnO_3$ powders synthesized by Pechini process and Figs. 3(c) and 3(d) show those obtained with the controlled precipitation method followed by slip casting. It is evident from Fig. 3 that samples show substantial porosity and that the grain size for the pieces formed with powders obtained by controlled precipitation, in some cases greater than 50 μm (Figs. 3(c) and (d), is larger than that of the pieces made with Pechini powders, slightly greater than 10 μm (Figs. 3(a) and (b)). The latter samples exhibit a more homogeneous microstructure. Table 1 show the microstructural dimensions and

characteristics of the pieces formed using ceramic powders synthesized by two distinct chemical pathways.

3.3. Electrical characterization

A complete circuit used to describe the electrical behavior should include electrodes and bulk effects, deep bulk traps, and grain boundaries, Figure 4 [17, 18].

The total capacitance dependence on frequency is strongly affected by the presence of deep bulk traps. More specifically, expected deep traps, with a distribution of activation energies, imply a distributed impedance element. A constant phase element (CPE) is a simple distributed element that reflects the microscopic material inhomogeneities, having a constant phase angle in the complex plane [19]. A CPE is an empirical impedance function of the following form

$$Z_{CPE} = \frac{1}{A(j\omega)^{\alpha}} \qquad (1)$$

The constant A determines the impedance modulus and the exponent α determine the impedance angle. In the special case of α=1, the CPE acts like a capacitor with A equal to the capacitance. The CPE can also behave as an inductance, α=-1, or a resistance, α=0. At low frequencies, the equivalent capacitance of the circuit of Fig. 4 is given by

$$C_p = C_{gb} + \frac{A.sen(\alpha\pi/2)}{\omega^{1-\alpha}} \qquad (2)$$

showing a slope that depends on the parameter α. At high frequency values, Eq. (2) reduces to

$$C_p\big|_{\omega\to\infty} = C_{gb}. \qquad (3)$$

In order to study grain boundary capacitance changes, we found that, in our case, for a frequency of 100 kHz, $C_p \approx C_{gb}$ (assuming that grains present Schottky potential barriers). Also, the electrode effects on total impedance and total capacitance, for our working frequency, can be neglected [20]. Thus, the

electrical capacitance behavior of the possible grain boundary barriers was analyzed at 100 kHz as a function of external bias, from 0 to 40 volts (see Fig. 5)

In Figure 5 it can be observed that grain size differences (see table I) do not directly correlate with changes of C_p (at 100 kHz) for samples S1, S2, and S3. However, a large electrical capacitance (C_p=C_{gb}) is observed for the controlled precipitation method when the samples (S4) are sintered at 1450 °C. Figure 5 also indicates mild capacitance dependence with bias for the Pechini method (S1 and S2) and controlled precipitation (S3). Conversely, S4 shows appreciable capacitance dependence with bias from 0 to 20 V. This dependence is another evidence of the grain boundary barriers formation in these grains. For no bias, grain boundary capacitance measurements are shown in Table 2.

With the information given in Table 1, we can calculate the capacitance considering that we are dealing with a homogeneous material:

$$C_{blocks} = \varepsilon_r \varepsilon_0 \frac{S}{d} \qquad (4)$$

where, ε_r=18 [21]. With Eq. (4) the experimental capacitance should be about 10 pF. A significantly larger value indicates the presence of intergranular potentials barriers and a bulk region at the center of the grains. The large capacitance value found in the 1450 °C blocks made using the controlled precipitation method constitutes strong evidence that this is the case in which potential barriers are not overlapped. Related with this, a lower resistance was observed in the full bias range for the precipitation method and it is shown in Figure 6.

In principle, the capacitance is inversely related to the distance between electrodes. For a homogeneous material, this is directly the thickness *d* as shown in Eq. 4. However, if Schottky barriers are developed at grain surfaces, *i.e.*, when potential barriers are not overlapped, the effective distance between electrodes is reduced. In a grain of size *z*, having two depletion regions of width L, every grain reduces their effective width to 2L. Thus, in a one dimensional approximation, the resulting capacitance when barriers are non–overlapped, C_{no}, related to that corresponding to a sample with overlapped barriers, C_o, can be expressed as [22]:

$$\frac{C_{no}}{C_o} = \frac{z}{2\Lambda} \qquad (5)$$

where z is the grain size and Λ is the depletion layer width. For the controlled precipitation method, following sintering, the capacitance of the $BaSnO_3$ blocks changes considerably in the explored sintering temperature range. Indeed, the ratio between the block capacitances at 1450 °C and at 1350 °C is ≈56, using the results of Figure 7 or Table 2. This change can be interpreted with Eq. (5) as the consequence of depletion widths that are narrower than the grain radius, due to a higher doping. From Eq.(5), considering that S4 has mostly non-overlapped barriers, the depletion layer can be estimated as

$$\Lambda = \frac{z}{2}\left(\frac{C_O}{C_{S4}}\right) \cong 1.19x10^{-7}\, m \qquad (6)$$

In a Schottky barrier, the height (ϕ and width (Λ) are directly related [20, 21]:

$$\phi = \frac{eN_d}{2\varepsilon}\Lambda^2 \qquad (7)$$

where N_d is the donor density. (Strictly, ϕ refers to band bending in Eqs. 7-10.) With Eq. (7) the donor concentration N_d can be estimated considering a typical values of barrier height of 0.65 eV (value that we will confirm below):

$$N_d = \frac{2\varepsilon\phi}{e\Lambda^2} \qquad (8)$$

The dopant concentration can also be determined considering the capacitance for n intergrains in series:

$$\frac{1}{C_{gb}} = 2\left(\frac{2\phi n^2}{e\varepsilon N_d S^2}\right)^{1/2} \qquad (9)$$

where ϕ is given in V. Equation (9) corresponds to the capacitance obtained from measurements shown in Fig. 7(a). N_d can be calculated from C_{gb} as:

$$N_d = C_{gb}^2 \phi \left(\frac{8n^2}{q\varepsilon_0 \varepsilon_r S^2} \right) \qquad (10)$$

With Eq. (10) the value for the dopant concentration can be determined, N_d=1.22x10^{23} m^{-3}, which is quite close to the one determined using Eq. (8). On another hand, results for capacitance values indicate that Schottky barriers do not develop for samples S1, S2, and S3. This implies very low-doped samples. Indeed, for having complete depleted samples, the dopant concentration in a spherical grain should be:

$$N_d \leq \frac{6\varepsilon\phi}{e\Lambda^2}$$

For a grain of 5 mm, this implies a $N_d \leq$6x10^{20} m^{-3}. This is a relatively low doping but this is expected because samples were sinterized and always exposed to air. Apparently, the sample preparation using controlled precipitation method favors the oxygen vacancy formation.

To gain confidence in the previous analysis based on capacitance measurements, we calculated the total current due to both tunnelling and thermionic emission. The total current density over and through a barrier can be calculated as:

$$J = \frac{AT}{k} \int_0^V f(E)P(E)dE + AT^2 \exp(-e\phi/kT) \qquad (11)$$

The first term corresponds to the tunneling current (**J$_{tunneling}$**) and the second to the thermionic current, *A* and *k* are the Richardson and Boltzmann constants respectively, *f*(*E*) is the Fermi-Dirac distribution and *P*(*E*) the transmission probability. The analysis leading to Eq.(11) can be extended to incorporate thermionic-field emission or tunneling contributions, which can be calculated using

$$J_{tunneling} = \frac{AT}{k} \int_0^{\phi} F(E)P(E)dE . \qquad \mathbf{(12)}$$

F(E) is the Fermi-Dirac distribution and *P(E)* is the transmission probability for a reverse-biased Schottky barrier, which can be determined by means of the Wentzel-Kramer-Brilloin (WKB)

approximation [17]. The experimental current density (J_{exp}) can be obtained from the grain boundary resistance (Fig. 7(b)) with the following relationship:

$$J = V / SR_{gb(20\,Hz)} \quad (\mathbf{13})$$

where V is the applied voltage during impedance spectroscopy measurements, S the block area (6.5×10^{-5} m^2) and R_{gb} the grain boundary resistance measured at low frequencies. Then, a pair of N_d and ϕ values was used for fitting experimental values with Eqs. 10–13. Iterative calculations were carried out until the calculated total current (thermionic and tunnel current) was equal to the experimental value obtained with Eq. (13), see Table 3 confirming our previous estimations. The study of the electrical behavior of the ceramic pieces was carried out at a temperature of 300 °C for two reasons. First, gas sensors present maximum sensitivity at about this temperature and, second, at room temperature the conductivity is some cases is too low to be measured and then comparisons are not possible.

In order to compare the two synthesis methods, the electrical capacitance and resistance response as functions of frequencies, at 300 °C and 0 Bias, for samples sintered at 1450 °C were measured (S2 and S4). These studies are presented in Figure 7(a), and Figure 7(b), respectively.

At low frequencies, the film electrical behavior can be described with the electrical model shown in Figure 4. In this circuit, the resistance R_{traps} and the CPE mimic the effect of deep traps **[23, 24]**. An increase in C_p (Figure 7(a)) at low frequencies is observed due to the presence of deep bulk traps in all samples. Moreover, Figure 7(b) shows that grain size differences cannot be responsible for the huge change in resistance. However, this can be interpreted as the formation of narrow intergranular barriers that facilitate conduction in the S4 sample.

4. Conclusions

The results obtained in this study indicate that the method of synthesis used to obtain the raw material as well as the method employed in forming the pieces determines the electrical behavior of the barium stannate block samples. The method used is then crucial for the resulting morphology and electrical properties. Depending on the preparation method, and then the donor concentration, intergranular potential barriers could be overlapped or not. For a large enough donor concentration, when barriers are non–overlapped, the electrical capacitance is relatively large due to the narrow depletion layers at

intergrains, which also facilitate conduction. Linked with this, the grain boundary electrical capacitance show dependence with the applied voltage as donor concentration is large.

5. Acknowledgements

The authors are grateful to VRI of the University of Cauca for project funding (ID 3587) and logistical support and to Colin McLachlan for suggestions related to the English text.

References

[1] Vorgelegt V, Wensheng L (2002) Synthesis of nanosized $BaSnO_3$ powders. Doctoral thesis in Engineering of Natural Sciences, Faculty of Engineering, University of Saarlandes, Saarbrücken–Alemania; pp. 1–2.

[2] Wensheng L, Helmut S (2008). Lyothermal synthesis of nanocrystalline $BaSnO_3$ powders. J Ceram Int 34, 645–649.

[3] Jarzebski ZM, Marton JP (1976) Physical properties of SnO_2 materials first part preparation and defect structure. J Elect Soc 7, 99–205.

[4] Cerdà J, Arbiol J, Dezanneau G, Díaz R, Morante JR (2002) Perovskite–type $BaSnO_3$ powders for high temperature gas sensor applications. J Sens Act B 84, 21–25.

[5] Cuervo–Farfán J, Arbey–Rodríguez J, Fajardo F, Vera–López E, Landínez–Téllez DA, Roa–Rojas J (2009) Structural properties, electric response and electronic feature of $BaSnO_3$ perovskite. J Phys B 404:2720–2722.

[6] Premakumara Udawatte C, Kakihana M, Yoshimura M (1998) Preparation of pure perovskite-type $BaSnO_3$ powders by the polymerized complex method at reduced temperature. J Sol St Ion 108, 23–30.

[7] Pugh RJ, Bergstrom L (1994) Surface and colloid chemistry in advanced ceramics processing. Surfactant science series, Vol. 151, Marcel Dekker Inc. New York.

[8] Serrini P, Briois V (1997) Chemical composition and crystalline structure of SnO_2 thin films used as gas sensor. Thin Solid Films 304, 13–122.

[9] Moreno–Botella R (2005) Rheology of ceramic slurries. Higher Council for Scientific Research, Madrid.

[10] Mistler RE, Twiname ER (2000) Tape Casting, theory and practice. Amer Ceram Soc. Westerville.

[11] Rahaman MN (2007) Ceramic processing. CRC Press – Taylor y Francis Group. Boca Raton.

[12] Tseng WJ, Wu ChH (2000) Aggregation, rheology and electrophoretic packing structure of aqueous Al_2O_3 nanoparticle suspensions. Act. Mater 50, 3757–3766.

[13] Tseng WJ, Lin K (2003) Rheology and colloidal structure of aqueous TiO_2 nanoparticle suspensions. Mat Sci Eng A 355, 186–192.

[14] Shen Z, Chen J, Zou H, Yun J (2004) Rheology of colloidal nanosized $BaTiO_3$ suspension with ammonium salt of polyacrylic acid as a dispersant. J Coll Surf A 244, 61–66.

[15] Khan AU, Hag AU, Mahmood N, Ali Z (2012) Rheological studies of aqueous stabilized nano–zirconia particle suspensions. J Mater Res 15 (1), 21–26.

[16] Ochoa–Muñoz YH, Ponce MA, Rodríguez-Páez JE (2015) Comparative study of two wet chemical methods of $BaSnO_3$ synthesis: Mechanism of formation of mixed oxide, Powder Technol., 279, 86–95.

[17] Rhoderick EH, Williams RH, *Metal-Semiconductor Contacts*, Oxford Science, 2nd edn., 1988, pp.35.

[18] Ponce MA, Castro MS, Aldao CM (2009) Capacitance and resistance measurements of SnO_2 thick–films. J Mater Sci: Mat Elec Springer Ed. 20, 25–32.

[19] Ross Macdonald J (1987) Impedance spectroscopy, emphasizing solid materials and systems. John Wiley & Sons Inc. publications, Canada.

[20] Ponce MA, Parra R, Savu R, Joanni E, Bueno PR, Cilense M, Varela JA, Castro MS (2009) Impedance spectroscopy analysis of TiO_2 thin film gas sensors obtained from water–based anatase colloids, Sens. Act. B, Vol. 139 (2), 447–452.

[21] CRC Handbook of Chemistry and Physics, 87th Ed. D. R. Lide. Boca Raton, FL; 2006; Ch.12, p. 44.

[22] F. Schipani, M. A. Ponce, E. Joanni, F. J. Williams, and C. M. Aldao (2014) Study of the oxygen vacancies changes in SnO2 polycrystalline thick films 2 using impedance and photoemission spectroscopies, Journal of Applied Physics 116, 194502.

[23] Chiou BS, Chung MC (1991). Admittance spectroscopy and trapping phenomena of ZnO based varistors. J. Elec Mater 20(7):885–890.

[24] Blatter G, Greuter F (1986) Electrical Brekdown at semiconductor grain boundaries. Phys Rev B 34(12):8555–8572.

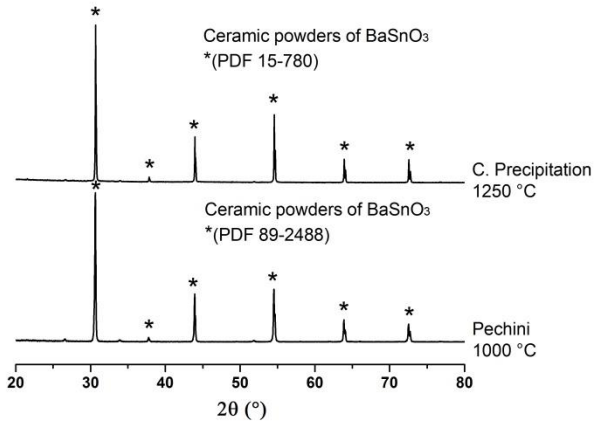

Figure 1. XRD graphs of the solid samples synthesized using controlled precipitation and Pechini routs; the powders were thermally treated for 2 hours at 1250 °C and 1000 ºC, respectively.

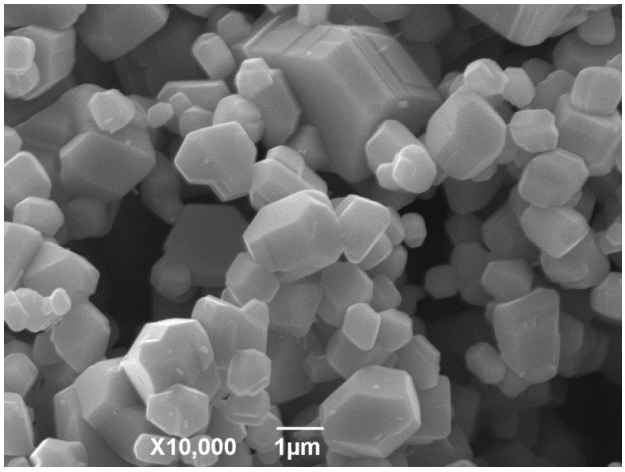

(a)

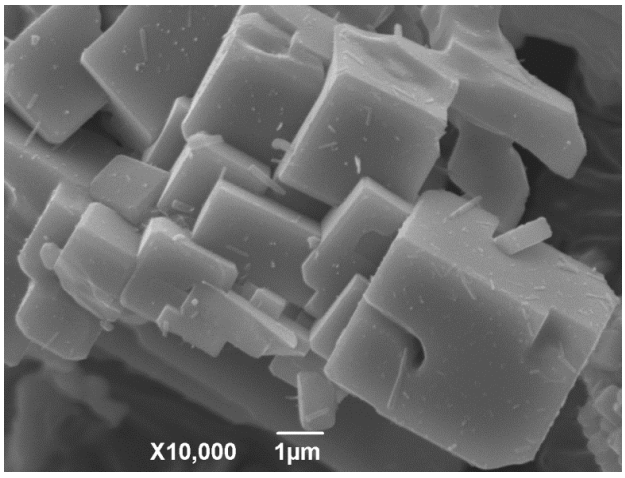

(b)

Figure 2. SEM images of $BaSnO_3$ powders synthesized using (a) controlled precipitation method (thermally treated at 1250 °C) and (b) Pechini polymeric precursor route (treated at 1000 °C).

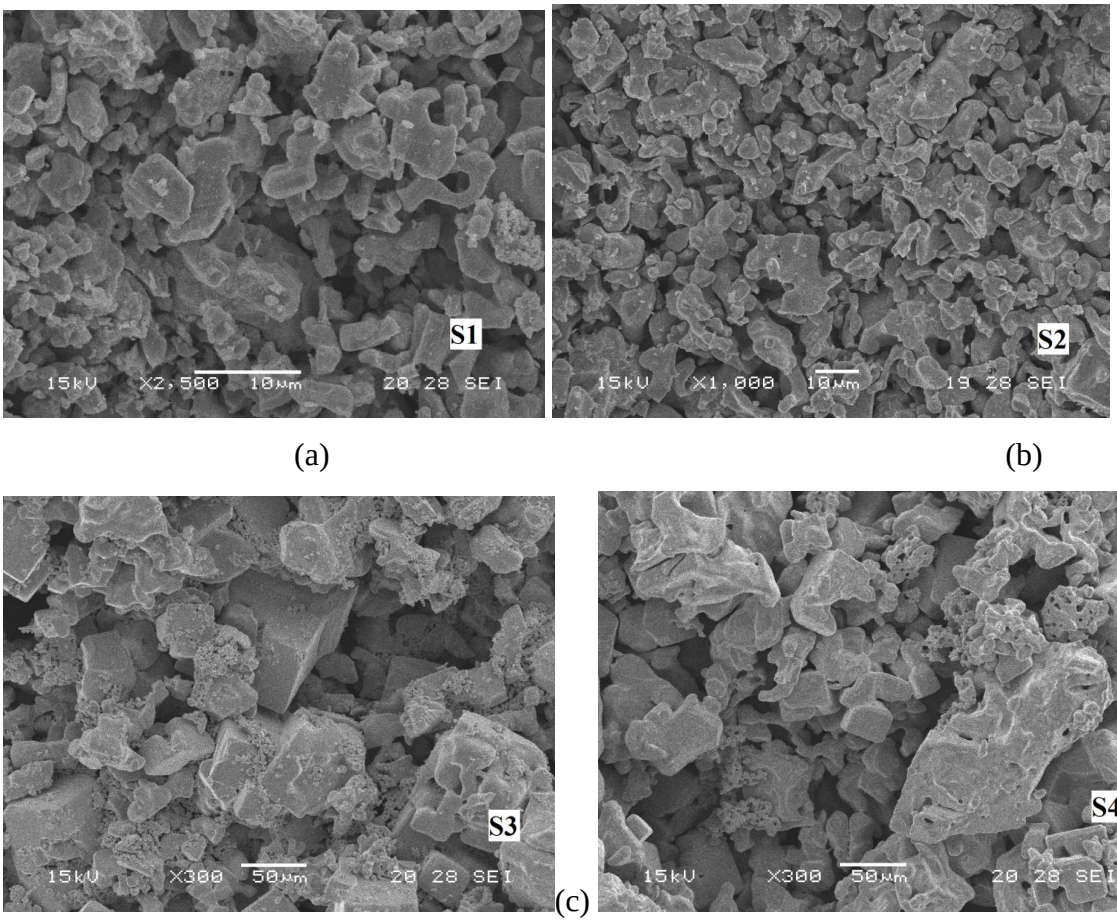

Figure 3. SEM images of the surface of the ceramic pieces formed by slip casting using powders synthesized with the Pechini method, sintered at (a) 1350 ºC labeled S1 and (b) 1450 ºC labeled S2, and synthesized with the controlled precipitation method, sintered at (c) 1350 ºC labeled S3 and (d) 1450 ºC labeled S4

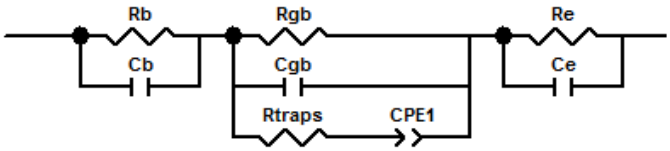

Figure 4. Equivalent circuit that includes four different contributions to the overall impedance (for the full frequency range): grain boundary, bulk, deep bulk traps, and electrode contact. R_{gb} and C_{gb} represent grain boundary resistance and capacitance, respectively. R_b and C_b represent bulk resistance and capacitance, respectively. The electrode elements are R_e and C_e, while a constant phase element (CPE) is used to model deep bulk traps.

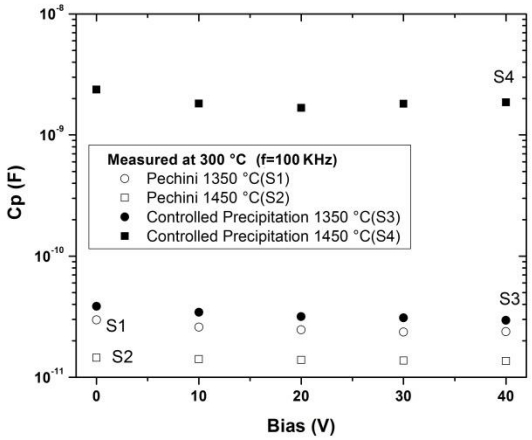

Figure 5. Capacitance as a function of applied bias for S1, S2, S3, and S4 samples.

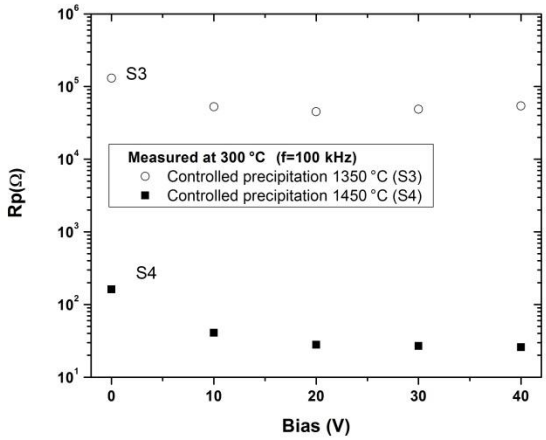

Figure 6. Resistance vs. bias for S3 and S4.

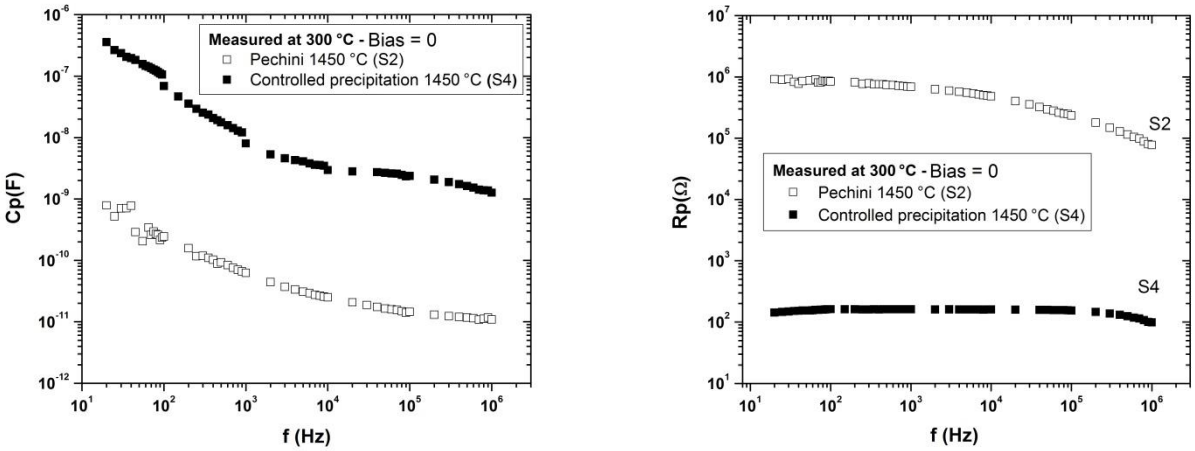

(a) (b)

Figure 7. Capacitance (a) and Resistance (b) as a function of frequency for the S2 and S4 samples.

Table 1. Microstructural characteristics of pieces formed using synthesized ceramic powders.

Structural measurements	Pechini		Controlled Precipitation	
	S1	S2	S3	S4
Sintering temperature (°C)	1350	1450	1350	1450
Contact Area "*S*"(m^2) x 10^{-5}	6.35	6.47	7.26	6.5
Block thickness "*d* " (mm)	1.05	1.3	1.35	1.2
Grain size "*z*" (μm)	5	10	30	30
No. of grains in thickness *d*	210	130	45	40

Table 2. Electrical Parallel Capacitance (C_p) at 100 kHz for different sintering temperatures.

Blocks measured at 0 bias	Pechini		Controlled precipitation	
Sintering temperature (°C)	S1=1350	S2=1450	S3=1350	S4=1450
(C_p at f=100 kHz) (pF)	12.4	10.9	22.6	C_{gb} =1260

Table 3. Electrophysics parameters obtained from the experimental measurements.

Blocks measured at 0 Bias	**Controlled precipitation**	
Sintered temperature (°C)	1350	1450
C_p (pF)	22.6	C_{gb} =1260
R_{gb} (kΩ)=R_p	131.101	0.142
J_{total} (A/m^2)	0.11	108.34
J_{tunnel} (A/m^2) (model)	Overlapped	~56
$J_{thermionic}$ (A/m^2) (model)	potential	~52
Barrier height eϕ (eV)	barriers	0.67
Donor concentration (1/m^3)	$C=\varepsilon S/d$	1.22x10^{23}
Depletion layer width (nm)	$J = V / SR_{gb(20Hz)}$	119